CDRD and PNPR passive microwave precipitation retrieval algorithms: extension to the MSG full disk area

G. Panegrossi, D. Casella, S. Dietrich, A. C. Marra, L. Milani, M. Petracca, P. Sanò, and A. Mugnai

Institute of Atmospheric Sciences and Climate/National Research Council (ISAC/CNR)

Area della Ricerca di Tor Vergata, Via del Fosso del Cavaliere 100, 00133 Rome, Italy

Abstract

Within the EUMETSAT H-SAF program (Satellite Application Facility on Support to Operational Hydrology and Water Management, http://hsaf.meteoam.it) we have developed two different passive microwave precipitation retrieval algorithms: one is the Cloud Dynamics Radiation Database algorithm (CDRD), based on a physically-based Bayesian approach for conically scanning radiometers (i.e., DMSP SSMIS); the other one is the Passive microwave Neural network Precipitation Retrieval (PNPR) algorithm for cross-track scanning radiometers (i.e., NOAA and MetOp-A/B AMSU-A/MHS). The algorithms originally created for Europe and the Mediterranean basin have been recently extended to Africa and Southern Atlantic for application to the MSG full disk area. The two algorithms are based on the same physical foundation, i.e., same cloud-radiation model simulations to be used as *a priori* information in the Bayesian solver and as *training* dataset in the neural network approach. They also use similar procedures for screening of non-precipitating pixels, identification of frozen background surface, detection of snowfall, and determination of a pixel based quality index of the surface precipitation retrievals. Operational precipitation products based on CDRD and PNPR covering the MSG full disk area will be soon made available within H-SAF. In this paper the methodology used to create a cloud-radiation database representative of the area of interest is described, as well as the changes made in the precipitation retrieval algorithms to account for the extended database. The results of a verification study over the African continent using as ground truth the TRMM Precipitation Radar will be shown. Future development of the algorithms for the full exploitation of the NASA/JAXA Global Precipitation Measuring mission (GPM) is also presented.

1. Introduction

With the recent advent of the NASA/JAXA Global Precipitation Measuring (GPM) mission (Hou et al., 2014) a new era has started for precipitation monitoring. The constellation of satellites carrying PMW radiometers has reached its optimal configuration, ensuring a 3-hourly global coverage, and the first spaceborne dual-frequency precipitation radar (DPR), along with the advanced GPM Microwave Imager, onboard the GPM core satellite, will be the reference instruments for precipitation retrieval providing consistency around the globe. Global monitoring of the precipitation requires the full exploitation of all overpasses of present and future satellites carrying cross-track and conically scanning passive microwave (PMW) radiometers orbiting around the globe and accurate, through consistent estimates of the precipitation among the different instruments. To this purpose it is necessary to refine and improve precipitation retrieval techniques and test their ability to retrieve precipitation from different sensors in all environmental and meteorological conditions. This will not only serve to the global monitoring of the precipitation, but also to promote and improve applications in hydrology, relying mostly on precipitation products based on the combined use of PMW precipitation estimates and GEO-IR observations.

Our interest is to develop accurate and consistent satellite precipitation products from the GPM constellation of satellites. Within the EUMETSAT H-SAF program (Satellite Application Facility on Support to Operational Hydrology and Water Management, http://hsaf.meteoam.it) we have developed two different passive microwave (PMW) precipitation retrieval algorithms (see Mugnai et al., 2013a for a description of all H-SAF precipitation products): one is the Cloud Dynamics Radiation Database algorithm (CDRD, Casella et al., 2013, Sanò et al., 2013a, Mugnai et al., 2013b), a physically-based Bayesian approach for conically scanning radiometers (i.e., DMSP SSMIS, GMI); the other one is the Passive microwave Neural network Precipitation Retrieval algorithm (PNPR, Sanò et al., 2013b, 2014, Mugnai et al., 2013b) for cross-track scanning radiometers (i.e., NOAA and MetOP-A/B AMSU-A/MHS, Suomi NPP ATMS).

A new version of the two algorithms have been recently delivered to retrieve precipitation over the full Meteosat Second Generation (MSG) area. The H-SAF cloud-radiation database, used as *a priori* information in the Bayesian solver and as *training* dataset in the neural network approach, originally created for Europe and for the Mediterranean basin, has been extended to Africa and Southern Atlantic. The two algorithms use dynamical/meteorological/environmental variables as ancillary information to characterize the observed event, and mitigate the ambiguity of the cloud microphysical structures (and rainfall rates at the ground) associated to any given set of measured multichannel brightness temperatures (TBs) (Smith et al., 2013, Casella et al., 2013). They are based on the same physical foundation, i.e., same cloud-radiation model simulations (Mugnai et al., 2013b). Operational precipitation products based on the extended versions of CDRD and PNPR will be soon available within H-SAF, for hydrological applications and for monitoring (in quasi-real time through precipitation products based on the combined use of PMW precipitation estimates and GEO-IR observations) drought and extreme events in regions with sparse rain gauge and radar network such as the African continent.

In this paper the two algorithms are briefly described, and the main features of the extended database are presented. The results of a validation study for the year 2011 and 2012 over the African continent using the Tropical Rainfall Measuring Mission (TRMM) Precipitation Radar (PR) as ground truth will be shown. The advantages of using the large set of consistent precipitation measurements in assessing the algorithm strengths/weaknesses and retrieval accuracy are discussed, and future development of the algorithms within H-SAF is outlined.

2. Description of the CDRD and PNPR algorithms

The H-SAF operational precipitation product for PMW conical scanning radiometers (identified as H01 in H-SAF) is a physically-based Bayesian precipitation retrieval algorithm funded on a new methodology called Cloud Dynamics and Radiation Database (CDRD). A thorough presentation of the CDRD methodology, attributes and performance is provided by a series of recent publications: Sanò et al. (2013a), Casella et al. (2013), Smith et al. (2013) and Mugnai et al. (2013b). The algorithm has been designed specifically for the Special Sensor Microwave Imager and Sounder (SSMIS), on board the U.S: DMSP F16, F17, F18, and F19 satellites (soon the data from the F19 satellites will be released to the public). The ECMWF global forecast model output at 0.5 degrees closest in time of the SSMIS overpass at each location, provides the optimal dynamical/thermodynamical/hydrological constraint parameters (DTH tags) to be associated to the SSMIS observations. The algorithm provides instantaneous precipitation rate, with indication of phase and quality flag, at 13.2 x 15.5 km^2 resolution consistent with the SSMIS high-frequency window channel spatial resolution.

The precipitation product for cross-track scanning radiometers (identified as H02 in H-SAF) is based on Artificial Neural Network (ANN) approach. The algorithm is the Passive microwave Neural network Precipitation Retrieval (PNPR) algorithm, presented in Mugnai et al. (2013b) and Sanò et al. (2013b), and described in detail by Sanò et al. (2014). The algorithm processes measurements from the AMSU-A and MHS (or AMSU-B) radiometers, currently on board the U.S. NOAA-18 and NOAA-19 and European MetOp-A and MetOp–B satellites. As input data, it incorporates TBs and various additional channel-derived variables (see Sanò et al, 2014, for details). In order to reduce ambiguity of the rainfall rate associated to a given set of measurements, other geophysical/geographical inputs (i.e., latitude, terrain height, surface type, season) guide the algorithm towards the solution. The pixel number along the scan is an additional input parameter, needed to determine the degree to which limb smearing has to be reduced, an effect produced by the changing atmospheric path length along the scan (the neural network itself performs this limb correction). A procedure for correcting damaged MetOp-A radiometric channels has been also introduced. A surface precipitation rate (with indication of phase and quality flag) is provided at the nominal resolution of MHS varying from 16 x 16 km^2 / circular at nadir to 26 x 52 km^2/ oval at scan edge.

Both algorithms are based on a large database of simulations produced using the Cloud Resolving Model (CRM) Non-hydrostatic Modeling System (NMS) (Tripoli, 1992) coupled to a Radiative Transfer Model (RTM) that relates CRM environments to expected top-of atmosphere PMW TBs for the radiometer used. The original dataset used for the H-SAF area (Europe and Mediterranean area) was made of 60 simulations of different precipitation events over the European area for the period between March 2006 - February 2007 taking into account the various climatic regions, types of precipitation and seasonal variations (for details see Smith et al., 2013, Casella et al., 2013). For the extension of the algorithms to the MSG full disk area, 34 more simulations have been added, representative of the climatology and precipitation systems characteristic of Africa and Southern Atlantic. The events have been selected on the basis of the Tropical Rainfall Measuring Mission (TRMM) Precipitation Radar (PR) observations (in particular the Rain Type flag and the Freezing level height) and on the basis of different climatic regions in order to cover as much as

possible the climatic variability in the area of interest with a limited number of simulations. Table 1 provides the list of all cases selected to generate the database for the African regions, while Fig. 1 shows the map of the spatial distribution of the inner domain of the 34 simulations over Africa.

#	Date	UTC time	Lat.	Lon.	Brief description
1	20/02/2007	00:00	-25,00	42,00	TrCy Favio (Madagascar)
2	21/08/2006	00:00	8,00	-15,00	tropical storm debby West Africa/Atlantic
3	23/07/2006	00:00	11,00	34,50	floods over Ethiopian highlands
4	03/06/2010	17:16	22,00	59,00	Tropical Cyclone phet (Oman)
5	17/07/2008	06:21	8,81	15,83	Storm over Nigeria-Ciad
6	18/06/2006	16:52	17,00	11,80	scattered precipitation Niger
7	02/08/2007	02:36	10,50	3,19	MCS Benin
8	20/09/2007	01:33	1,50	20,14	MCS NW Congo - fast growing
9	03/10/2007	20:49	-21,44	26,52	NE Botswana storm after front
10	07/04/2007	14:30	-22,65	45,64	Madagascar (orographic)
11	09/10/2007	03:40	-1,00	25,00	MCS line Congo
12	26/05/2006	23:26	32,50	-3,00	Storm over Atlas
13	29/01/2006	15:22	24,50	6,00	MCS Sahara Algeria
14	10/12/2006	04:01	-26,70	31,00	Storm Swaziland
15	11/04/2006	17:30	-3,70	0,70	MCS Guinea Gulf
16	19/03/2007	23:49	-3,50	14,00	MCS WestCentral
17	15/07/2006	19:41	14,00	-8,00	MCS Sahel
18	21/04/2007	01:13	32,50	-6,00	Storm front North Morocco
19	20/01/2006	17:02	32,80	-24,00	Storm North Atlantic Ocean
20	14/10/2007	15:19	2,19	-11,63	Mixed Guinea Gulf
21	13/05/2006	01:01	8,61	25,50	Stratiform-Convective Sud Sudan
22	05/04/2006	20:04	22,94	48,33	Stratiform-Convective Saudi Arabia
23	05/02/2006	22:06	-26,11	22,19	Stratiform-Convective Botswana
24	18/03/2007	01:41	-11,90	12,17	Stratiform-Convective Angola coast
25	16/11/2007	04:20	-32,65	-25,08	Shallow-warm line South Atlantic
26	06/08/2007	23:50	-16,25	49,99	Shallow-warm Madagascar
27	29/01/2006	05:41	16,98	39,43	Shallow-warm Red Sea
28	10/05/2007	03:27	-34,90	20,35	Shallow-warm line South Africa
29	16/02/2006	23:18	18,49	-5,36	Stratiform Sahara Mauritania
30	30/03/2007	13:35	31,52	21,85	Stratiform Lybia NE
31	16/12/2006	23:07	-12,70	25,96	Stratiform round Zambia
32	29/01/2007	00:20	-10,55	37,44	Stratiform Tanzania
33	25/10/2006	22:09	8,65	43,62	Stratiform Ethiopian Highlands
34	22/09/2006	15:05	-2,10	59,49	Stratiform intense N-Indian Sea

Table 1: List of all simulations used to generate the African/Southern Atlantic database

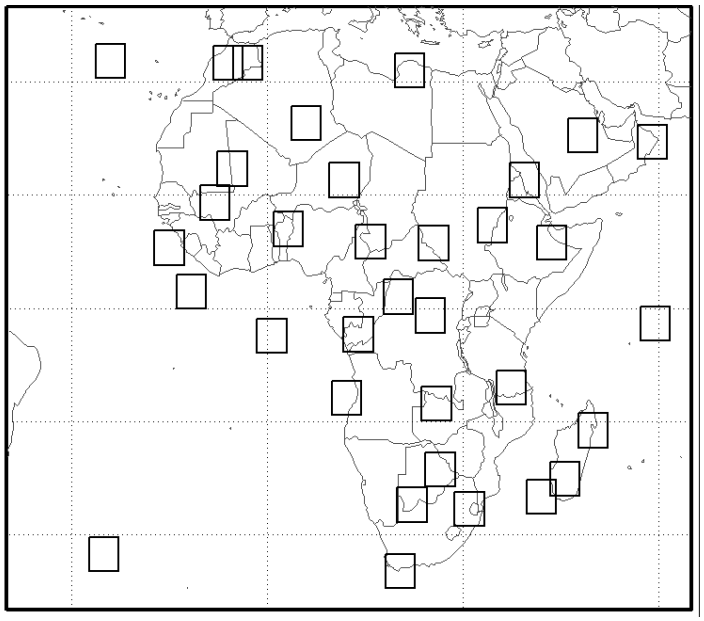

Fig. 1: Spatial distribution of the NMS inner domain of the 34 NMS simulations over the African region

Every vertical profile generated by the model at high resolution is used to generate a plane-parallel precipitating environment, to which the radiative transfer model (Eddington approximation) is applied to compute the upwelling TBs at the different incident viewing angles of the radiometers, i.e., 1 constant viewing angle for SSMIS, or 45 different angles for AMSU-A/MHS. The simulated TB's are then spatially averaged using the radiometer Gaussian antenna pattern functions varying with channel frequency and viewing angle. This means that the PNPR database is 45 times larger than the CDRD database (which itself contains some 5 million entries). The surface emissivity model (for ocean, vegetated land, and frozen soil) is described in Casella et al. (2013), while for arid land (desert) the model uses the TELSEM emissivity atlas (see Prigent et al., 2006).

For the seek of consistency between PMW H-SAF precipitation products deriving from cross-track and conically scanning radiometers the same screening algorithm of not-precipitating pixels is used in the two algoritms. Over all background surfaces except over desert (vegetated land, ocean, snowy/frozen background, coast) the screening of not-precipitating pixels is based on the methodology described in Mugnai et al. (2013b). For the Arid Land pixels the screening is based on a Canonical Correlation Analysis (CCA) approach described in detail by Casella et al. (2014). The procedures used to determine both the phase and the quality index are similar in the CDRD (for H01 H-SAF product) and PNPR (for the H02 H-SAF product). The quality index is based on four different criteria: 1) Quality of input data (sensor used, horizontal resolution, presence of corrupted channels); 2) Background surface; 3) Event type; 4) Retrieval performance (i.e., the Bayesian variance of the retrieval in CDRD, viewing zenith angle across the scan for PNPR). The phase flag is based on the studies on snow and ice detection (see Mugnai et al., 2013b for details). It is evaluated only for pixels flagged as precipitating after the screening procedure and it is not available for pixels where coast is present in the background surface.

3. Dataset description

The validation of H01 (CDRD) and H02 (PNPR) precipitation products was carried out in the area between 36°S - 36°N in latitude and 60°E-60°W in longitude, covering the African continent, part of the Arabian Peninsula, part of the Southern American continent and part of the Atlantic and Indian Ocean. All the analysis was performed considering coincident observations of the Tropical Rainfall Measuring Mission (TRMM) precipitation Radar (PR) with observations from SSMIS and AMSU/MHS radiometers in the years 2011 and 2012. The TRMM-PR is the first spaceborne precipitation radar that has been recently declared no longer operational and can be considered the precursor of GPM DPR. It is a 13.8 GHz radar scanning between -17° and +17° with a swath width of 247 km (after the satellite was boosted at higher orbit in 2001). SSMIS is a conical scanning radiometer with an observation angle of 53.1 degrees, with a swath width of 1700 km, measuring passive microwave radiation in 24 channels with frequencies ranging from 19 to 183 GHz. The 19, 37 and 91 GHz channels are both in the vertical and horizontal polarization while the 22 and 150 GHz channels are present only in the horizontal polarization as the channels in the oxygen

absorption band (50.3-60.8 GHz) and in the water vapor absorption band (around 183.31 GHz). The SSMIS radiometer is carried onboard 4 satellites of the Defense Meteorological Satellite Program (DMSP) the F16, F17, F18 and F19; the launch of F20 satellite is planned for 2020. AMSU-A and MHS are both cross track sensors onboard 4 satellites NOAA-18, NOAA-19, MetOp-A and MetOp-B. AMSU-A has 23 channels between 23.8 and 89 GHz while MHS has one channel at 89 GHz, one at 157 GHz and 3 channels in the water vapor absorption band. The polarization measured by every channel changes with the scan angle which varies between -48° and 48°, and the swath width of the radiometer is around 1920 km.

We selected all available coincidences (considering a 15 minutes time window) of the SSMIS radiometer with the TRMM PR in the area of interest considering the DMSP-F16, DMSP-F17 and DMSP-F18 satellites (i.e. the ones available in the years considered). The same was done for the available AMSU/MHS radiometers considering MetOp-A, NOAA-18, and NOAA-19 satellites. Two datasets have been created, one of SSMIS-PR coincidences and one of AMSU/MHS-PR coincidences, with a total of 5247 and 2149 coincident overpasses for the AMSU/MHS and for the SSMIS dataset respectively. To obtain co-located vectors of SSMIS or AMSU/MHS brightness temperatures (TBs) and PR rainfall estimates (TRMM product 2A25), there are important issues to be considered: the parallax error between PMW radiometers and TRMM PR, and the fact that horizontal resolution changes with frequency in conically scanning MW radiometer (SSMIS) and with the observation angle in the cross-track scanning radiometers (AMSU/MHS). Moreover there are sampling differences between AMSU-A and MHS and between the SSMIS components (Imager, Environmental, Lower and Upper Atmospheric Sounder). First a partial correction of the parallax error was carried out to account for the differences in the observation geometry between SSMIS or AMSU/MHS and TRMM-PR and to account for the spatial shifts in the retrieved rainfall patterns at the surface especially true for deep convective clouds (see Casella et al., 2014 for details). Then, the TRMM-PR rainfall rate at the surface was downscaled to the SSMIS and MHS nominal resolution, defined as the IFOV size of the 91 GHz / 89 GHz channel for the SSMIS / MHS radiometer respectively. All the channels with a coarser spatial grid were re-sampled using a nearest neighbor approach, and for the AMSU-A/MHS sensors we have considered an IFOV size variable with the scan angle as described by Bennartz (2000).

The resulting datasets were divided into 3 classes depending on the background surface as: Land, Ocean and Coast using a digital land/sea map at 2 seconds of arc resolution. Then the Land class was subdivided into Vegetated Land and Arid Land (desert). The arid land pixels have been identified looking at the mean annual difference of the DMSP SSMIS 19 GHz V and H channels (Grody, 1991). One year (2011) of SSMIS observations has been used. Figure 2 shows the results of this procedure. It is clear how the Sahara desert and the Arabian desert have been correctly identified as arid land. Smaller areas of arid land also appear in Iran (including the Dasht-e Kavir and the Dasht-e lut deserts) and in the African continent (including the Kalahari desert in South-West Africa and arid regions in the continental Horn of Africa). However some small deserts near to the coast have been not correctly identified, i.e. the Namib Desert in Namibia and the Danakil Desert in the African coast of the Red sea. The Coast pixels have been excluded from this test to eliminate the polarization difference due to the sea surface emissivity.

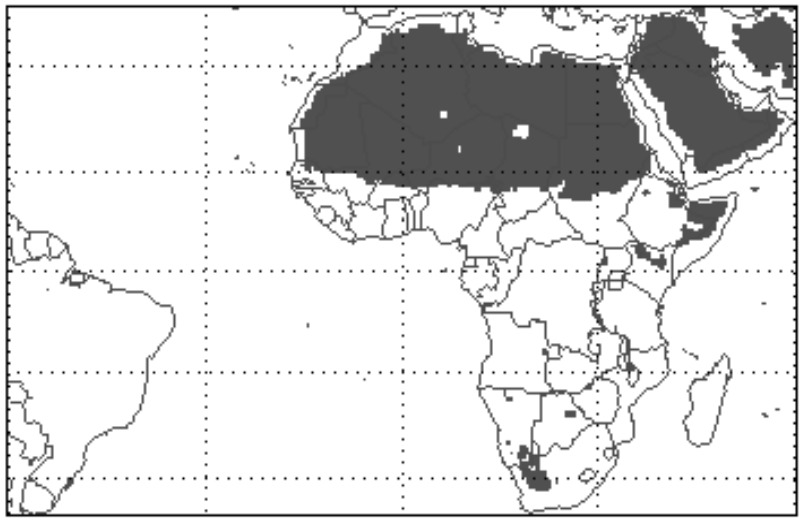

Fig. 2: Map of areas identified as desert or arid land in the study area (36°S - 36°N - 60°E-60°W).

4. Results

Figure 3 shows an example of the H-SAF H01 rainfall rate (RR in mm/h), obtained from the CDRD algorithm, for the MSG full disk area. The precipitation rate is obtained from the SSMIS overpass of Jan 20, 2012, at 1521 UTC. The SSMIS overpass captures tropical cyclone Funso off the coast of Mozambique on 19 January 2012. The TRMM PR precipitation rate at 1550 UTC is also shown for comparison.

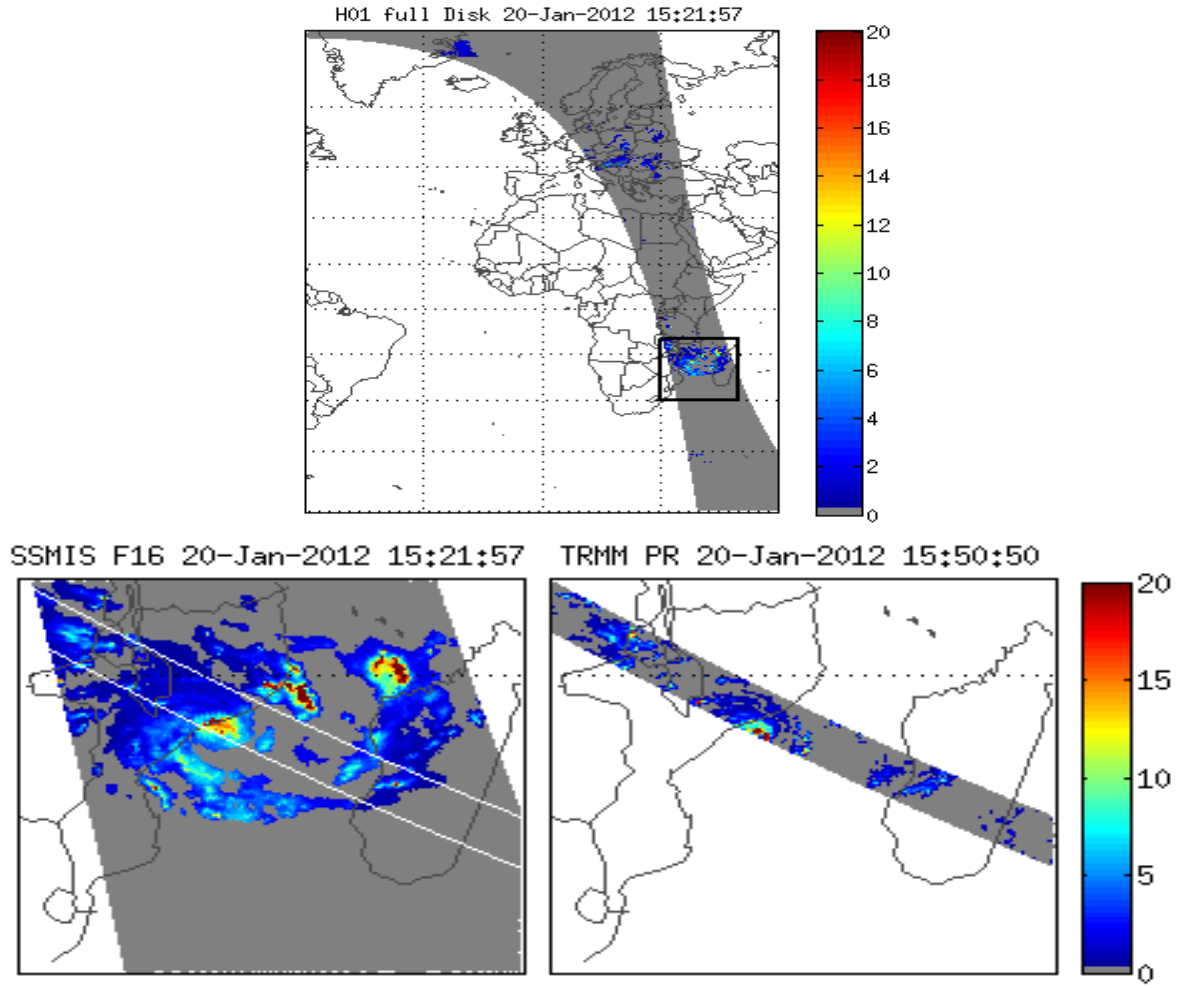

Fig. 3: H01 Rainfall rate (mm/h) obtained from the CDRD algorithm over the MSG full disk area (top) for SSMIS (F16) overpass on January 20, 2012 1521 UTC. Detail over Madagascar and Mozambique of tropical cyclone Funso (bottom left) and TRMM PR (2A25 product) overpass on the same area at 1550 UTC (bottom right).

Figure 4 shows an example of the H-SAF H02 rainfall rate for the MSG full disk area (obtained from the PNPR algorithm) for the AMSU/MHS (MetOp-A) overpass on January 6, 2012 over Mozambique and Madagascar. The MHS TB at 157 GHz is also shown. Both algorithms delineate quite well the precipitation, and the most intense convective cores of precipitation areas are very well identified.

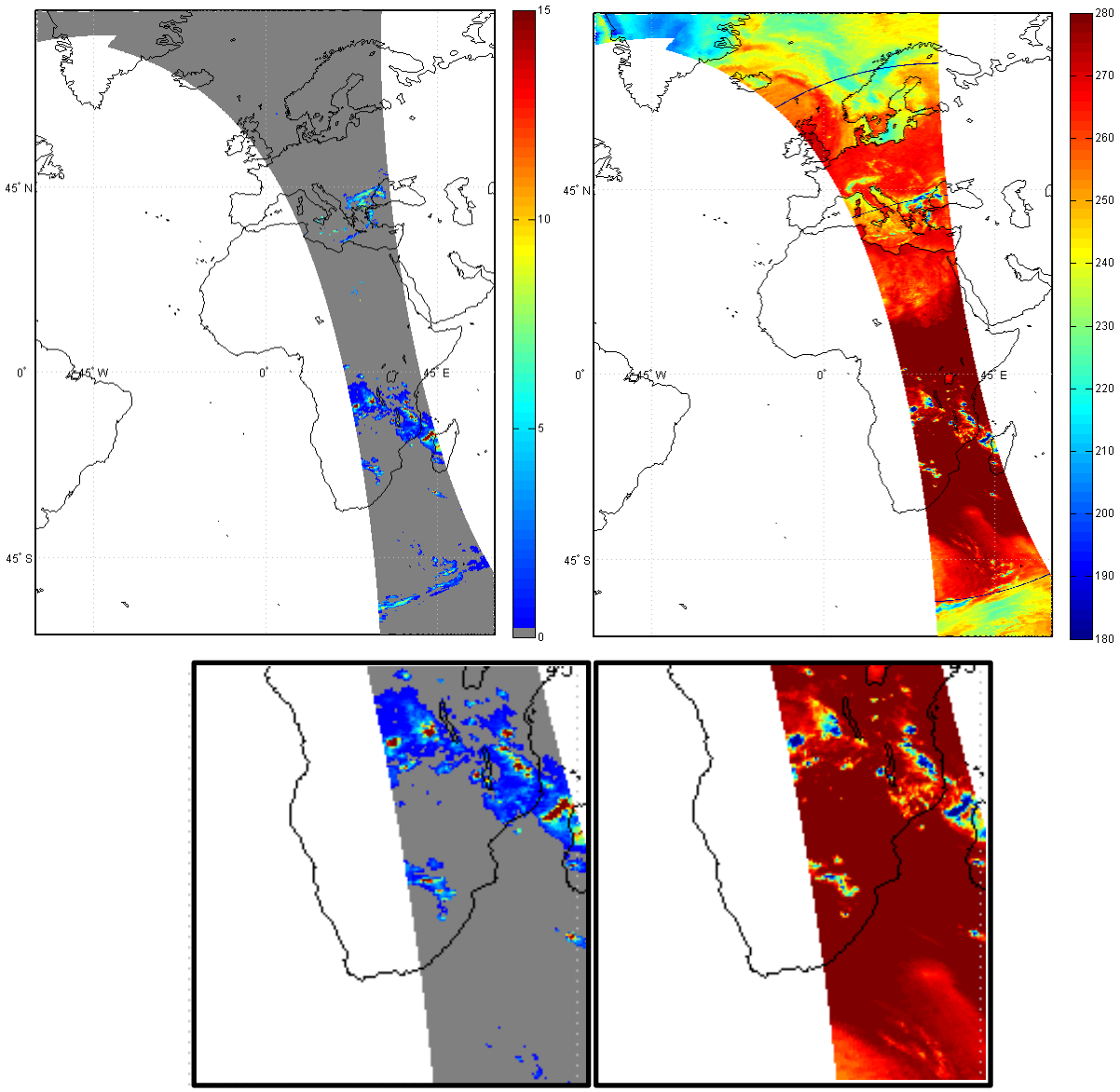

Fig. 4: H02 Rainfall rate [mm/h] obtained from the PNPR algorithm over the MSG full disk area (top left) for AMSU/MHS (MetOp-A) overpass on January 6, 2012 1809 UTC, and the MHS TB at 157 GHz [K] (top right). Zoom over Madagascar and Mozambique of rainfall rate (bottom left) and TB at 157 GHz (bottom right).

The statistical scores have been evaluated for the two full datasets (SSMIS-PR coincidences for the H01 H-SAF product, and AMSU/MHS-PR coincidences for the H02 H-SAF product) over 2011-2012. The analysis has been carried out for the different types of background surfaces (vegetated land, arid land, ocean, coast) and for four different classes of precipitation (no rain, very light, light/moderate, heavy).

Table 2 shows the contingency table obtained for the full 2011-2012 dataset of H02 PNPR and TRMM PR (2A25) coincidences, and for the different types of surface. Over all surfaces there is a very good ability of the algorithm to screen out the not precipitating pixels (similar results are obtained for H01). However, the very light precipitation is often missed. The algorithm shows good ability to retrieve light/moderate precipitation, while the heavy precipitation (> 10 mm/h) is sometimes underestimated. Table 3 shows the statistical scores for the different types of surface. The scores show a quite good agreement between H02 and PRMM PR 2A25 product with values of CC ranging between 0.58 for desert and 0.71 for coastal areas, a RMSE between 1.91 and 2.21 mm/h, and a ME between 0.08 and 0.21 mm/h.

Figure 5 shows the results for the full dataset (only for rainy pixels according to the TRMM-PR, i.e., RR ≥ 0.25 mm/h) where the binning analysis proposed by Ferraro and Marks (1995) has been carried out. The TRMM-PR 2A25 RR has been sampled in 1 mm/h size bins to calculate the mean "*true*" RR in each bin; the mean H02 rainfall rate of the corresponding pixels have been computed for each bin. Figure 5 shows the scatterplot of the H02 binned mean RR vs. the mean TRMM-PR RR in each bin. The figure shows also the

variability of the Fractional Standard Error (FSE) as a function of the mean TRMM-PR RR, where FSE (%) is defined as:

$$FSE\% = 100\ \frac{RMSE}{\overline{true}}$$

and $\overline{true}$ is the mean TRMM PR RR in each bin.
The analysis shows very good agreement for RR < 10 mm/h, slightly worse results for higher RR. Overall the CC is 0.87, and the RMSE is 1.93 mm/h. The FSE is lower than 100% for RR > 7 mm/h, and it reaches 300% for very low RR values. These results are remarkably good also considering that the analysis has been carried out at the H02 product nominal resolution, and not on a regular grid at coarser resolution as done in Tang et al. (2014). It is worth noting that in Tang et al. (2014) the binning analysis of precipitation retrieval over the U.S. from cross-track scanning radiometer AMSU/MHS (downscaled to a 0.25ºx0.25º regular grid), carried out using high quality radar estimates (Q2 product) from the U.S. National Mosaic and Multi-Sensor QPE (NMQ) system as ground-truth, shows worse results in terms of adjusted RMSE% than those shown in Fig. 5 (much higher than 300% for RR < 1 mm/h) and in terms of CC (between 0.45 in the winter and 0.6 in the summer).

Total	**< 0.25 (No rain)**	**0.25≤ Rad < 1.0**	**1.0≤ Rad < 10.0**	**Rad ≥10.0**
< 0.25 (No rain)	**98.3%**	**70.2%**	32.1%	2.5%
0.25≤ Sat < 1.0	0.7%	6.4%	6.2%	1.3%
1.0≤ Sat < 10.0	0.9%	21.9%	**50.6%**	**49.3%**
Sat ≥10.0	0,0%	1.4%	11.0%	47.0%
Land	**< 0.25 (No rain)**	**0.25≤ Rad < 1.0**	**1.0≤ Rad < 10.0**	**Rad ≥10.0**
< 0.25 (No rain)	**98%**	**56.8%**	22.7%	2.0%
0.25≤ Sat < 1.0	1.3%	15.3%	11.4%	2.5%
1.0≤ Sat < 10.0	0.6%	26.9%	**55.7%**	**48.0%**
Sat ≥10.0	0.0%	0.9%	10.1%	47.4%
Coast	**< 0.25 (No rain)**	**0.25≤ Rad < 1.0**	**1.0≤ Rad < 10.0**	**Rad ≥10.0**
< 0.25 (No rain)	**97,8%**	**68.2%**	37.6%	1.5%
0.25≤ Sat < 1.0	1.3%	8.7%	5.9%	0.0%
1.0≤ Sat < 10.0	0.9%	22.2%	**47.6%**	27.7%
Sat ≥10.0	0.0%	0.8%	8.9%	**70.8%**
Ocean	**< 0.25 (No rain)**	**0.25≤ Rad < 1.0**	**1.0≤ Rad < 10.0**	**Rad ≥10.0**
< 0.25 (No rain)	**98.4%**	**78.8%**	42.5%	2.9%
0.25≤ Sat < 1.0	0.3%	0.8%	0.5%	0.0%
1.0≤ Sat < 10.0	1.2%	18.7%	**45.0%**	**51.8%**
Sat ≥10.0	0.0%	1.6%	12.1%	45.2%
Arid Land	**< 0.25 (No rain)**	**0.25≤ Rad < 1.0**	**1.0≤ Rad < 10.0**	**Rad ≥10.0**
< 0.25 (No rain)	**99.6%**	**71.6%**	32.8%	4.3%
0.25≤ Sat < 1.0	0.1%	4.0%	3.3%	0.0%
1.0≤ Sat < 10.0	0.3%	23.4%	**51,4%**	**54.3%**
Sat ≥10.0	0.0%	0.9%	12,5%	41.3%

Table 2: Contingency table for the four types of background surfaces and for four precipitation classes for the 2011-2012 coincidence dataset of H02 product (PNPR algorithm) and TRMM-PR 2A25 product.

The analysis of the results of H01 (CDRD algorithm) for the SSMIS/TRMM PR dataset of coincidences for 2011-2012 is under evaluation. The results obtained for the H02 product with the PNPR algorithm for cross-track scanning radiometer AMSU/MHS are remarkably good especially considering the all statistical scores have been evaluated at the radiometer nominal spatial resolution and not on a regular coarser grid. Similar results were obtained for a verification study carried out over Europe, where both the H01 (based on CDRD) and H02 (based on PNPR) products were analyzed for 22 case studies, and were compared with ground-based radar and rain gauge measurements provided by the H-SAF Precipitation Product Validation team (see Panegrossi et al., 2013, Sanò et al., 2014). In that case, however, the major difficulty in assessing the quality of the satellite-based precipitation retrievals consisted in taking into account the variable quality of the data used as ground-truth, and the evident lack of homogeneity among the datasets provided by the different European countries. In the study presented in this paper, the large set of consistent precipitation measurements over such a large area provided by the TRMM PR adds value to the assessment of the algorithm strengths and weaknesses and of the retrieval accuracy. Since March 2014, such kind of datasets for precipitation retrieval validation are being provided globally by the GPM DPR and will be used in the future for verification of the PMW precipitation products that are being developed within H-SAF.

	Land	**Ocean**	**Coast**	**Arid Land**
Total number of pixels	1182872	1019600	31120	328301
ME	0,14	0,21	0,146	0,08
RMSE	2,21	2,19	2,09	1,91
SD	2,23	2,22	2,1	1,92
CC	0,64	0,62	0,71	0,58

Table 3: Global statistical scores for the four types of background surfaces for the 2011-2012 coincidence dataset of H02 product (PNPR algorithm) and TRMM-PR 2A25 product.

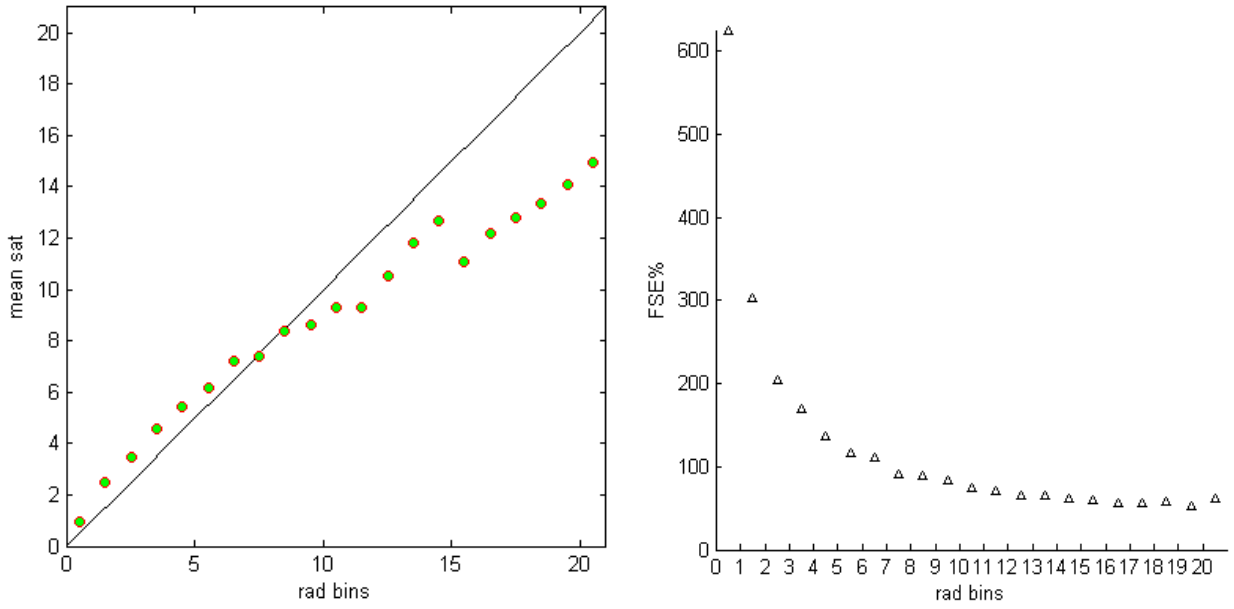

Fig. 5: Mean PNPR retrieved values reported as a function of the 1 mm/h rain rate bins of the corresponding TRMM-PR 2A25 estimates (left) (CC = 0.87, RMSE = 1.93 mm/h) and Fractional Standard Error percentage (FSE%) values obtained for each bin as a function of the 1 mm/h rain rate bins (right)

5. Conclusions

Our goal in developing H-SAF precipitation products from PMW radiometers on board the available LEO polar orbiting satellites is to achieve accurate, and consistent estimate of the precipitation among the different sensors. To this purpose it is necessary to refine and improve precipitation retrieval techniques, and test their ability to retrieve precipitation from the different sensors in all environmental and meteorological conditions. This will not only serve to the global monitoring of the precipitation, but also to promote and improve applications in hydrology, relying mostly on precipitation products based on the combined use of PMW precipitation estimates and GEO-IR observations. In this study we have described the new versions of the H01 and H02 precipitation products extended to the MSG full disk area, based respectively on the CDRD and PNPR retrieval algorithms. These two products are respectively designed for the conical scanning SSMIS radiometer, and for the cross-track scanning AMSU/MHS radiometers. The validation study carried out over the African region for the years 2011 and 2012 using the TRMM PR precipitation estimates as ground-truth has shown good abilities of the algorithms to screen out the not precipitating areas over the different types of background surface (including desert), good ability to retrieve light to moderate precipitation (1 mm/h ≤ RR < 10 mm/h), and heavy precipitation (RR ≥10 mm/h), while there is a tendency not to correctly identify very light precipitation (0.25 mm/h ≤ RR < 1 mm/h). Overall, the results obtained for H02 in terms of RMSE, CC, ME, and FSE are remarkably good (H01 results are under evaluation).

In order to optimally exploit the potentialities of the GPM constellation of satellites for optimal temporal and spatial coverage for precipitation monitoring (with direct improvement of all precipitation products based on combined MW/IR techniques), we aim at delivering precipitation products for *all* available PMW sensors. In the near future new products optimized for the European/Mediterranean areas (H-SAF area) as well as for the other regions of interest in the H-SAF project (i.e., Africa and Southern Atlantic) will be delivered for all the radiometers in the GPM constellation, including the conical scanning G-COMW1 AMSR-2, the cross-track scanning Suomi NPP ATMS, and the GPM Microwave Imager (GMI).

Acknowledgements

This work has been supported by the EUMETSAT H-SAF. We wish to thank the NASA Goddard Earth Sciences (GES) Data and Information Services Cewnter (DISC) Distributed Active Archive Center (DAAC) for providing TRMM PR 2A25 data, and the NOAA National Climatic Data Center (NCDC) for providing the SSMIS and AMSU/MHS data.

References

Bennartz, R.: Optimal convolution of amsu-b to amsu-a, J. Atmos. Ocean. Tech., 17, 1215–1225, 2000.

Casella, D., Panegrossi, G., Sano, P., Dietrich, S., Mugnai, A., Smith, E. A., Tripoli, G. J., Formenton, M., Di Paola, F., and Leung, W.-Y.: Transitioning from CRD to CDRD in Bayesian retrieval of rainfall from satellite passive microwave measurements: Part 2. Overcoming database profile selection ambiguity by consideration of meteorological control on microphysics, IEEE T. Geosci. Remote, 51, 4650–4671, 2013.

Casella, D., Panegrossi, G., Sanò, P., Milani, L., Petracca, M., and Dietrich, S.: A novel algorithm for detection of precipitation in tropical regions using PMW radiometers, Atmos. Meas. Tech. Discuss., 7, 9237-9274, doi:10.5194/amtd-7-9237-2014, 2014.

Hou, A. R. K. Kakar, S. Neeck, A. A. Azarbarzin, C. D. Kummerow, M. Kojima, R. Oki, K. Nakamura, and T. Iguchi, 2014: The Global Precipitation Measurement Mission. *Bull. Amer. Meteor. Soc.*, **95**, 701–722.

Ferraro, R. R. and Marks, G. F.: The development of SSM/I rain-rate retrieval algorithms using ground-based radar measurements, J. Atmos. Ocean. Tech., 12, 755–770, 1995.

Grody, N. C.: Classification of snow cover and precipitation using the Special Sensor Microwave Imager, J. Geophys. Res.-Atmos. (1984–2012), 96, 7423–7435, 1991.

Mugnai, A., Casella, D., Cattani, E., Dietrich, S., Laviola, S., Levizzani, V., Panegrossi, G., Petracca, M., Sanò, P., Di Paola, F., Biron, D., De Leonibus, L., Melfi, D., Rosci, P., Vocino, A., Zauli, F., Pagliara, P., Puca, S., Rinollo, A., Milani, L., Porcù, F., and Gattari, F.:: Precipitation products from the Hydrology SAF, Nat. Hazards Earth Syst. Sci., 13, 1959-1981, doi:10.5194/nhess-13-1959-2013, 2013a.

Mugnai, A., Smith, E. A., Tripoli, G. J., Bizzarri, B., Casella, D., Dietrich, S., Di Paola, F., Panegrossi, G., and Sanò, P.:, CDRD and PNPR satellite passive microwave precipitation retrieval algorithms:

EuroTRMM/EURAINSAT origins and H-SAF operations, Nat. Hazards Earth Syst. Sci., 13, 887-912, doi:10.5194/nhess-13-887-2013, 2013b.

Panegrossi, G., Casella, D., Dietrich, S., Sanò, P., Petracca, M., and Mugnai, A.: A Verification study over Europe of AMSU/MHS and SSMIS passive microwave precipitation retrieval, Proc. 2013 Joint EUMETSAT/AMS Meteorological Satellite Conference, 8 pp., 2013.

Prigent C, Aires F, Rossow WB.: Land surface microwave emissivities over the globe for a decade. Bull. Am. Meteorol. Soc. 87: 1573–1584. DOI:10.1175/BAMS-87-11-1573, 2006.

Sanò, P., Casella, D., Mugnai, A., Schiavon, G., Smith, E. A., and Tripoli, G. J., Transitioning from CRD to CDRD in Bayesian retrieval of rainfall from satellite passive microwave measurements, Part 1: Algorithm description and testing, IEEE Trans. Geosci. Remote Sens., Vol. 51, no. 7, 4119-4143, doi: 10.1109/TGRS.2012.2227332, 2013a

Sanò P. et al., Passive microwave Neural network Precipitation Retrieval (PNPR): an algorithm for cross-track scanning radiometers , *Proc. 2013 EUMETSAT/AMS Meteorol. Sat. Conference*, Vienna, Sept. 2013b

Sanò, P., Panegrossi, G., Casella, D., Di Paola, F., Milani, L., Mugnai, A., Petracca, M., and Dietrich, S.: The Passive microwave Neural network Precipitation Retrieval (PNPR) algorithm for AMSU/MHS observations: description and application to European case studies, Atmos. Meas. Tech. Discuss., 7, 9351-9411, doi:10.5194/amtd-7-9351-2014, 2014.

Smith, E. A., Leung, H. W.-Y., Elsner, J. B., Mehta, A. V., Tripoli, G. J., Casella, D., Dietrich, S., Mugnai, A., Panegrossi, G., and Sanò, P.: Transitioning from CRD to CDRD in Bayesian retrieval of rainfall from satellite passive microwave measurements: Part 3 – Identification of optimal meteorological tags, Nat. Hazards Earth Syst. Sci., 13, 1185-1208, doi:10.5194/nhess-13-1185-2013, 2013.

Tang, L., Y. Tian, and X. Lin, Validation of precipitation retrievals over land from satellite-based passive microwave sensors, J. Geophys. Res. Atmos., 119, 4546–4567, doi:10.1002/2013JD020933, 2014

Tripoli G. J., (1992) A Nonhydrostatic Mesoscale Model Designate to Simulate Scale Interaction, Mon. Weather Rev., 1 , 1342-1359.